Arch. Metall. Mater. **70** (2025), 2, 1113-1117

DOI: https://doi.org/10.24425/amm.2025.154452

SEUNGHEON HAN[1], HEE YEON JEON[1], JEONG HYUN KIM[1],
MYEONGJUN JI[2], GUN-JAE LEE[3], YOUNG-IN LEE[1*]

DIRECT SYNTHESIS OF DEFECTIVE TUNGSTEN TRIOXIDE MICROSPHERES USING ULTRASONIC SPRAY PYROLYSIS PROCESS FOR ENHANCED PHOTOTHERMAL CONVERSION PERFORMANCE

Defective tungsten trioxide (WO_{3-x}) is promising as a photothermal conversion material. However, WO_{3-x} prepared by conventional reduction of WO_3 suffers from limited photothermal efficiency due to oxygen vacancies forming mainly on the surface. In this study, we directly synthesized WO_{3-x} microspheres with a high concentration of oxygen vacancies using a modified ultrasonic spray pyrolysis (USP) method. Unlike conventional processes, this process can increase the concentration of oxygen vacancies in WO_{3-x} by adding an organic antioxidant to the precursor solution and applying an oxygen-free atmosphere. To systematically investigate the impact of these modifications, WO_3 or WO_{3-x} powders were synthesized using three USP conditions: a typical process, a process in an anoxic atmosphere, and a process combining both an anoxic atmosphere and an antioxidant. The resulting powder, with a distinct dark navy color indicating a high oxygen vacancy concentration, showed the most excellent light absorption, the lowest reflectivity, and the smallest band gap energy. This powder achieved the highest temperature increase under various light sources, demonstrating its superior photothermal conversion efficiency.

Keywords: Photothermal conversion; WO_{3-x}; oxygen defect; ultrasonic spray pyrolysis

1. Introduction

The photothermal effect is a physical phenomenon whereby a material absorbs light energy and converts it into thermal energy. Effective photothermal materials require a broad light absorption spectrum, high absorption rate, and superior photothermal conversion efficiency [1,2]. Depending on the application, factors such as toxicity, stability, and durability are also important considerations. The photothermal effect finds applications in diverse fields, including photothermal therapy, photothermal sterilization, and solar-driven water evaporation systems [3-7]. Photothermal materials are generally categorized into metal, carbon-based, polymeric, and semiconductor materials.

Among them, transition metal oxide semiconductors, such as WO_3, have attracted great attention as they offer a lower-cost synthesis route with high physicochemical stability under intense light and heat, and their hydrophilic properties make them well-suited for various photothermal conversion applications [8-10]. However, conventional WO_3 has a wide band gap of approximately 2.8 eV, primarily in the ultraviolet range, resulting in high absorption. In contrast, absorption efficiency remains low in the visible and near-infrared regions, restricting its use in sunlight-driven applications. Introducing oxygen vacancies is essential for the practical application of WO_3 to create new energy levels that narrow the band gap energy [11,12]. These oxygen vacancies can also induce localized surface plasmon resonance (LSPR), enhancing its optical response [13]. Therefore, incorporating oxygen vacancies in WO_3 represents a highly effective strategy to increase absorption abilities in the visible and near-infrared regions.

WO_{3-x} with oxygen vacancies is generally prepared by already synthesizing WO_3. It then uses a reduction process that removes oxygen in its lattice using hydrogen under high pressure or a strong reducing agent such as $NaBH_4$ [13]. However, this method can only cause oxygen vacancies on the surface and nearby regions, limiting its ability to improve photothermal conversion efficiency.

This study demonstrates the novel direct synthesis of WO_{3-x} microspheres with maximized oxygen vacancy concentration using ultrasonic spray pyrolysis (USP). A typical USP process

[1] SEOUL NATIONAL UNIVERSITY OF SCIENCE AND TECHNOLOGY, DEPT. OF MATERIALS SCIENCE AND ENGINEERING, SEOUL 01811, REPUBLIC OF KOREA
[2] UNIVERSITY OF NEVADA, DEPT. OF MECHANICAL ENGINEERING, LAS VEGAS, NV 89514, UNITED STATES OF AMERICA
[3] DEPT. OF CARBON NEUTRALITY AND CORPORATE GROWTH SUPPORT, KOREA PLANNING & EVALUATION INSTITUTE OF INDUSTRIAL TECHNOLOGY, DAEGU 41069, REPUBLIC OF KOREA

* Corresponding author: youngin@seoultech.ac.kr

uses ultrasonic waves to spray a solution containing a metal salt, and the resulting droplets are thermally decomposed in an air or oxygen atmosphere to synthesize spherical oxide powders continuously for a short period [14,15]. We established a strategy to maximize the oxygen vacancy concentration in WO_{3-x} microspheres by introducing an antioxidant into the precursor solution and changing the process atmosphere to nitrogen. The modified USP can form the crystal structure of WO_3 during the crystallization process in the pyrolysis step while minimizing the amount of oxygen that constitutes the lattice. To determine the effects of the antioxidant and nitrogen atmosphere on introducing oxygen vacancies in WO_{3-x}, powders were synthesized using the presence or absence of an antioxidant in the precursor solution and the process atmosphere controlled by oxygen and nitrogen, respectively. The particle size, shape, and crystal structure of the synthesized products were systematically analyzed, along with the optical properties and photothermal conversion efficiency.

2. Experimental

The precursor solution for synthesizing WO_{3-x} microspheres was prepared by dissolving 100 mM ammonium metatungstate hydrate (≥85% WO_3 basis, Sigma-Aldrich) and 1 M acetylacetone (AA, ≥99.5%, Sigma-Aldrich) in distilled water, and the addition of AA was set as a variable. The prepared solution was supplied at a 1.2 ml/min flow rate and atomized into fine droplets using a 1.7 MHz ultrasonic vibrator. The sprayed droplets were transported to a high-temperature tube furnace by oxygen or nitrogen carrier gas (2 L/min), and the temperatures at the bottom and top of the tube furnace were set to 200°C and 800°C, respectively, to induce solvent evaporation and thermal decomposition and crystallization of the precursor. The powder synthesized by the USP process was collected using filter paper. The powders synthesized under oxygen, nitrogen, and nitrogen atmospheres with antioxidants were named Y-WO_3, C-WO_{3-x}, and N-WO_{3-x}, respectively.

The shape and size of the synthesized powder were observed using FE-SEM (JSM-6700F, JEOL, Japan), and the crystal structure was analyzed using XRD (X'Pert Powder, Malvern Panalytical, Netherlands). In addition, the interatomic bonding energy was confirmed using XPS (K-Alpha, Thermo Fisher, UK). A Raman spectrometer (DXR Raman Microscope, Thermo Scientific, USA) measured the molecular vibrational structure. The reflectance and absorbance were measured using an ultraviolet-visible spectrometer (UV-2600i, SHIMADZU, Japan), and the band gap was calculated using the Kubelka-Munk function. The photothermal conversion performances of the powders were observed using an infrared lamp (PAR38E 230V 150W, PHILIPS, Netherlands), an 808 nm laser, and a solar simulator (DXP500, DY-Tech, Korea) as light sources to observe the temperature change of the powder.

3. Results and discussion

Fig. 1(a) shows FE-SEM images and colors (insets) of powders synthesized with the USP. The color of the powders showed a significant difference depending on the presence or absence of antioxidants in the precursor and the pyrolysis atmosphere. The Y-WO_3 and C-WO_{3-x} powders were yellow and cyan, respectively, and the N-WO_{3-x} powder was dark navy. This difference is due to the oxygen vacancies generated during the crystallization process. As the oxygen vacancies increase, a wider wavelength in the visible light range is absorbed more, which can show a darker color. The shape and particle size of the powders did not show a significant difference depending on the process conditions, and they were confirmed to be spherical particles with a particle size distribution of approximately 500 nm to 2 μm, which is the typical size and shape of powders synthesized with USP [16]. The surface roughness of the synthesized particles was observed, indicating that primary particles of several tens of nanometers in size were aggregated during pyrolysis to form relatively coarse spherical secondary

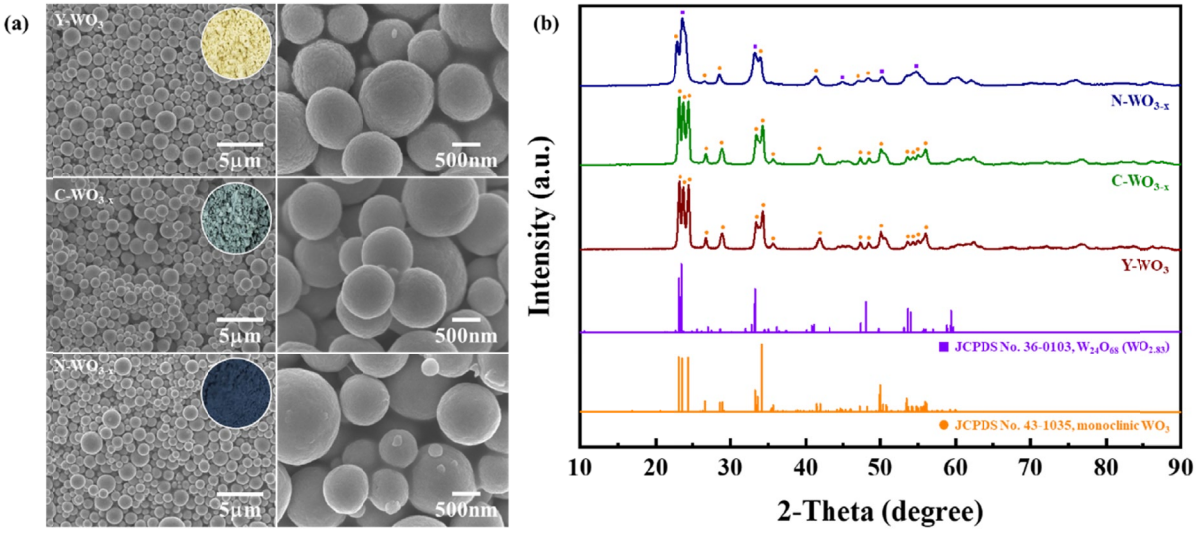

Fig. 1. (a) FE-SEM images and (b) XRD patterns of Y-WO_3, C-WO_{3-x}, and N-WO_{3-x} microspheres synthesized by USP at 800°C

particles. The crystal structure of the synthesized powder was confirmed by XRD analysis, and the analysis results are shown in Fig. 1(b). The Y-WO_3 and C-WO_{3-x} powders were confirmed to have a monoclinic WO_3 crystal structure. On the other hand, the N-WO_{3-x} powder simultaneously observed the diffraction patterns of monoclinic WO_3 and the non-stoichiometric phase of $W_{24}O_{68}$, confirming that a more considerable amount of oxygen vacancy was generated.

XPS and Raman analyses were performed to confirm whether oxygen vacancies were formed in each powder. Fig. 2(a) shows the XPS results for the synthesized WO_3 or WO_{3-x} microspheres. The binding energy of W 4f and O 1s of the Y-WO_3 powder showed the typical binding energy of WO_3 [17,18]. On the other hand, the C-WO_{3-x} and N-WO_{3-x} powder indicated positive shifts in both W 4f and O 1s, and the latter showed the most significant positive shift. This shift was caused by an increase in oxygen vacancies, which was in good agreement with the results reported in previous literature [17,18]. Fig. 2(b) shows the Raman spectrum of the synthesized powders. In the case of the Y-WO_3 powder, the peaks for the stretching vibration of the O-W-O bond were observed at 806 cm^{-1} and the bending vibration at 275 cm^{-1}, consistent with the typical Raman spectrum of WO_3 [19]. The Raman peaks of C-WO_{3-x} became broader, weaker, and redshifted. Moreover, the N-WO_{3-x} powders showed the most significant broad, weak, and redshifted. This difference is attributed to the disordered and non-stoichiometric bulk regions formed by introducing oxygen vacancies [19]. The Y-WO_3 powder can be considered pure WO_3 based on the XRD, XPS, and Raman results. In contrast, the C-WO_{3-x} and N-WO_{3-x} powders were identified as WO_{3-x} with oxygen vacancies. In addition, it can be seen that the case where an antioxidant was introduced contains a higher fraction of oxygen vacancies.

Fig. 3(a) shows the UV-Vis reflectance of the synthesized WO_3 and WO_{3-x} microspheres. Y-WO_3 (max. reflectance: about 60%) exhibited a typical reflectance spectrum of WO_3, which shows high reflectance in the visible and IR regions due to the unique band gap of WO_3. However, C-WO_{3-x} (max. reflectance: about 60%) and N-WO_{3-x} showed low reflectance in the visible and IR regions, indicating high absorption, and in particular, N-WO_{3-x} showed a low reflectance of less than 5%. This dramatic change in reflectance is attributed to the introduction of oxygen vacancies. As previously reported, the increase in oxygen vacancy concentration can improve the optical absorption properties of WO_3 by creating an intermediate energy band in the forbidden region, enabling electron excitation at low photon energies [11,12]. In addition, localized surface plasmon resonance (LSPR) can be generated by the collective vibration of carriers through the large number of free carriers formed by oxygen vacancies, which can improve light absorption near the NIR region [13,20]. Figure 3(b-d) shows the Kubelka-Munk plot obtained using the reflectance spectra of each powder, and the calculated band gap energies were drawn from the plot. Y-WO_3 was confirmed to have a band gap energy of 2.91 eV. On the other hand, C-WO_{3-x} and N-WO_{3-x} showed band gap energies of 2.84 eV and 2.43 eV, respectively, which were narrowed by oxygen vacancies. The band gap narrowing observed in this study (from 2.91 eV in Y-WO_3 to 2.84 eV and 2.43 eV in C-WO_{3-x} and N-WO_{3-x}, respectively) aligns well with previously reported results from various synthesis methods. Specifically, WO_{3-x} nanosheets synthesized via hydrothermal processes showed band gaps in the range of 2.25-2.60 eV, and those produced through chemical reduction exhibited approximately 2.49 eV [21,22]. In particular, in the case of N-WO_{3-x}, strong light absorption at about 2.0 eV (620 nm) can be observed, which can be explained by the LSPR effect due to the large number of oxygen vacancies.

Fig. 4 shows IR camera images showing the photothermal effect of the powders under various light sources. The N-WO_{3-x} microsphere showed the highest temperature under all light sources, while the Y-WO_3 showed the lowest temperature. One reason for the high photothermal conversion temperature of the N-WO_{3-x} was the increased recombination of electron-hole pairs formed by absorbed photons based on the improved visible light absorption by the abundant oxygen vacancies in the N-WO_{3-x}. Another reason was that the oxygen vacancies formed in the N-WO_{3-x} can introduce many free carriers and increase light absorption near the NIR region due to the LSPR generated when the density of free carriers exceeds a certain threshold.

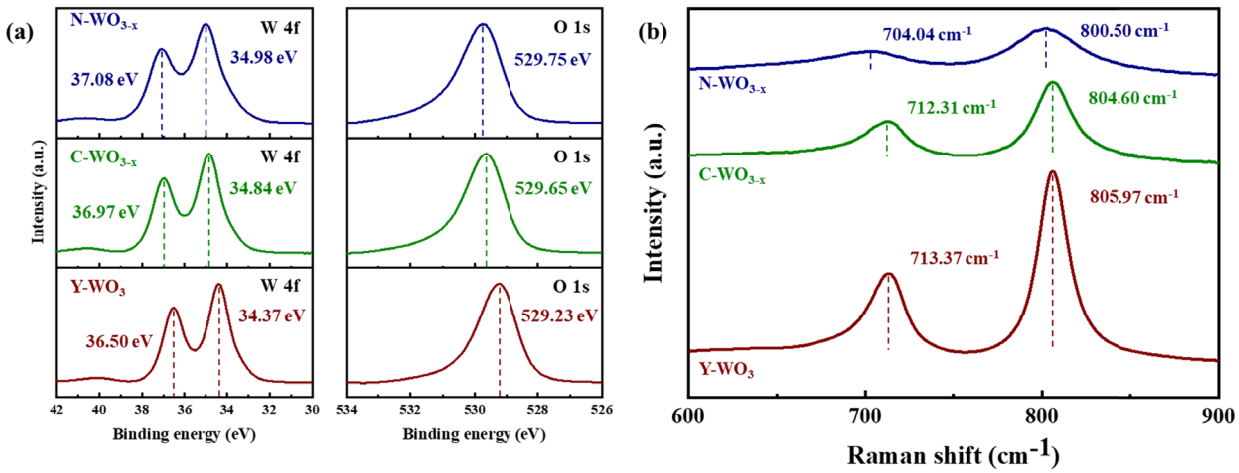

Fig. 2. (a) XPS and (b) Raman spectra of Y-WO_3, C-WO_{3-x}, and N-WO_{3-x} microspheres synthesized by USP at 800°C

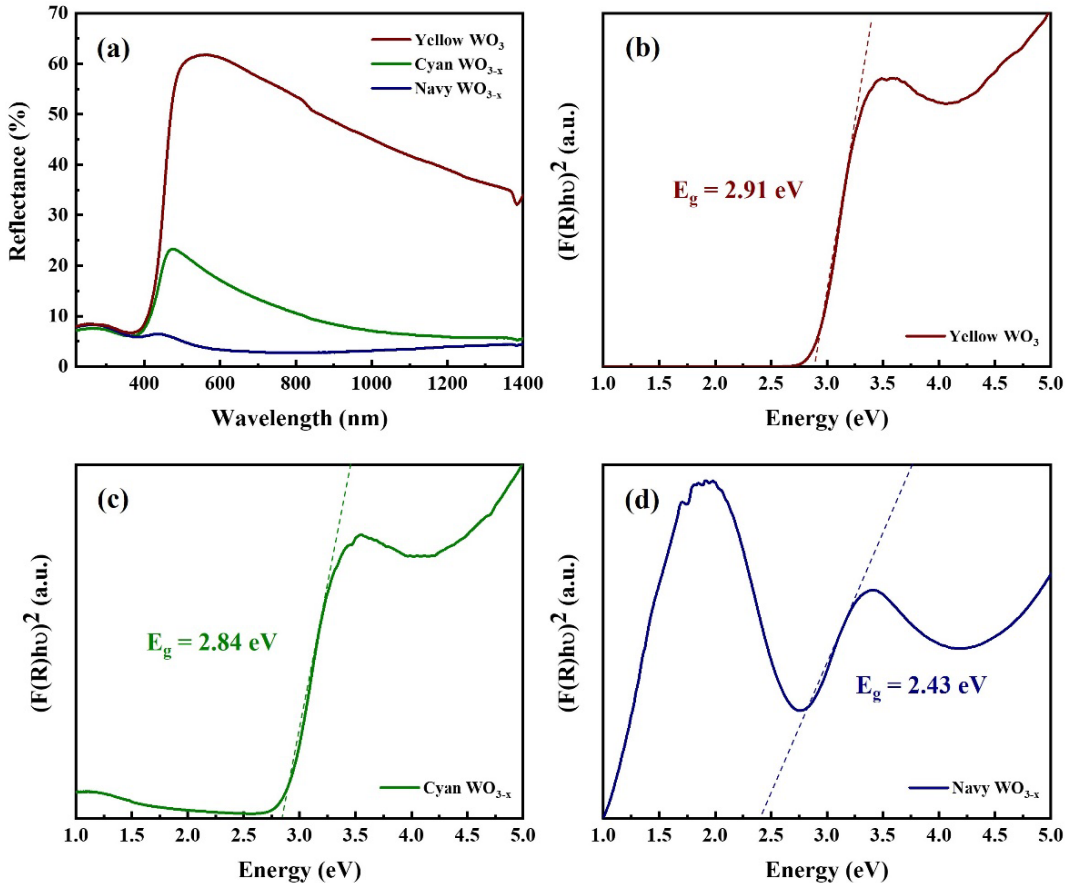

Fig. 3. (a) UV-Vis reflectance spectra and (b-d) Kubelka-Munk plots of (b) Y-WO_3, (c) C-WO_{3-x}, and (d) N-WO_{3-x} microspheres synthesized by USP at 800℃

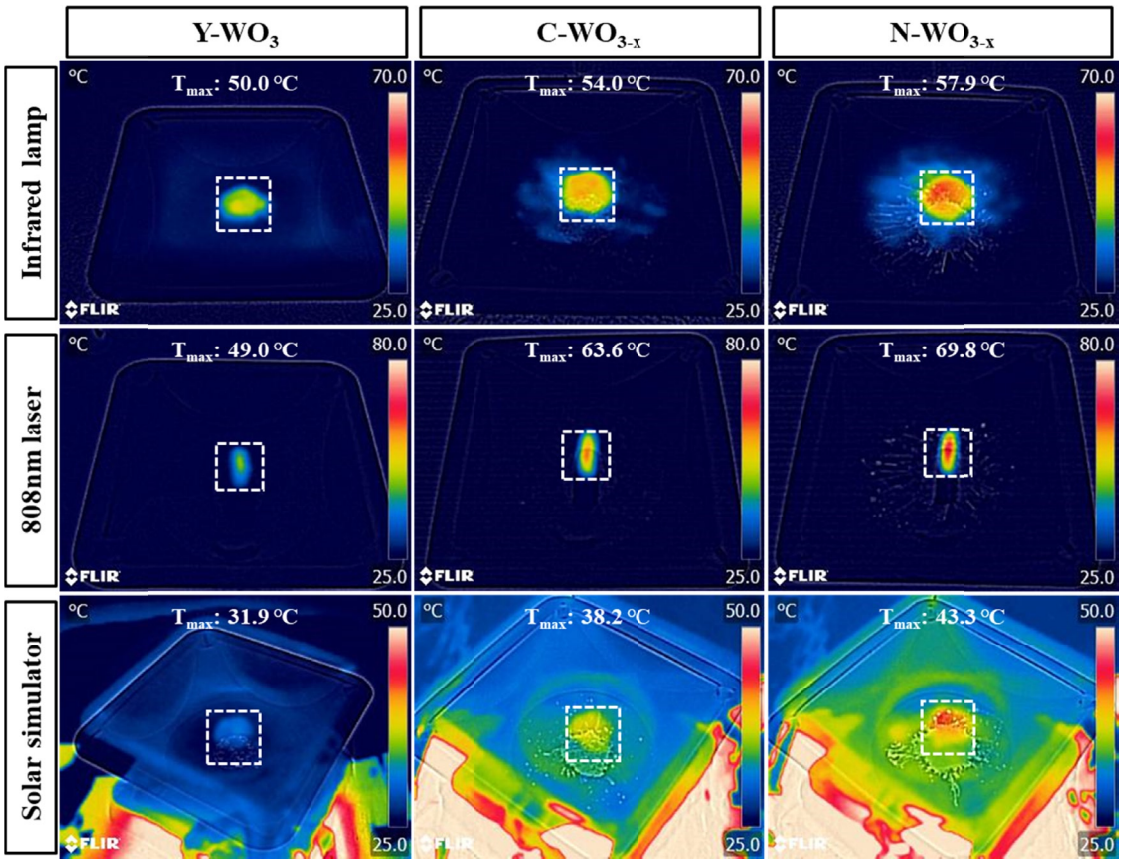

Fig. 4. IR camera images of Y-WO_3, C-WO_{3-x}, and N-WO_{3-x} microspheres synthesized by USP at 800℃ under various light sources

4. Conclusion

In conclusion, this study demonstrated the successful synthesis of WO_{3-x} microspheres with a high concentration of oxygen vacancies using USP under an N_2 atmosphere with an antioxidant additive. Oxygen vacancies in WO_{3-x} were confirmed through changes in color, crystal structure, binding energy shifts in XPS, and Raman spectra modifications. The enhanced oxygen vacancy concentration achieved by this direct synthesis approach resulted in reduced reflectance in the visible and IR regions, indicating increased light absorption and a narrowed band gap for N-WO_{3-x} (2.43 eV) and showing strong absorption near 620 nm due to the LSPR effect. Among the synthesized powders, N-WO_{3-x} exhibited the highest photothermal conversion efficiency, attributed to improved visible light absorption and increased carrier density facilitating LSPR. Thus, the modified USP method presents a promising and efficient approach for producing photothermal materials with enhanced light absorption and conversion capabilities suitable for diverse applications.

Acknowledgments

This work was supported by the National Research Foundation of Korea (NRF) grant funded by the Korea government (Ministry of Science and ICT) (NRF-2022R1A2C1011616).

REFERENCES

[1] X. Cui, Q. Ruan, X. Zhuo, X. Xia, J. Hu, R. Fu, Y. Li, J. Wang, H. Xu, Chemical Reviews **123**, 11 (2023).

[2] P. Cheng, D. Wang, P. Schaaf, Advanced Sustainable Systems **6**, 9 (2022).

[3] H. Ma, M. Xue, Journal of Materials Chemistry A **9**, 33 (2021).

[4] R. Xiong, F. Sauvage, J.C. Fraire, C. Huang, S.C. De. Smedt, K. Braeckmans, Accounts of Chemical Research **56**, 6 (2023).

[5] J.W. Xu, K. Yao, Z.K. Xu, Nanoscale **11**, 18 (2019).

[6] F. Zhao, Y. Guo, X. Zhou, W. Shi, G. Yu, Nature Reviews Materials **5**, 5 (2020).

[7] X. Wu, Y. Lu, X. Ren, P. Wu, D. Chu, X. Yang, H. Xu, Advanced Materials (2024).

[8] K.W. Tan, C.M. Yap, Z. Zheng, C.Y. Haw, P.S. Khiew, W.S. Chiu, Journal of photochemistry and photobiology C: Photochemistry Reviews **9**, 1 (2008).

[9] B. Yang, Z. Zhang, P. Liu, X. Fu, J. Wang, Y. Cao, R. Tang, X. Du, W. Chen, S. Li, H. Yan, Z. Li, X. Zhao, G. Qin, X. Q. Chen, L. Zuo, Nature **22**, 7983 (2023).

[10] R. Watanabe, C. Fukuhara, H. Yamashita, P. Verma, Catalysis Science & Technology **14**, 17 (2024).

[11] M.B. Johansson, B. Zietz, G.A. Niklasson, L. Österlund, Journal of Applied Physics **115**, 21 (2014).

[12] F. Zhan, Y. Liu, K. Wang, X. Yang, M. Liu, X. Qiu, J. Li, W. Li, ACS Applied Materials & Interfaces **11**, 43 (2019).

[13] R. Watanabe, C. Fukuhara, H. Yamashita, P. Verma, Catalysis Science & Technology **14**, 17 (2024).

[14] M. Ji, J.H. Kim, H.Y. Jeon, S. Han, D.H. Lee, Y.-I. Lee, Chemical Engineering Journal **483**, 149435 (2024).

[15] B.H. Min, K.Y. Jung, Journal of Korean Powder Metallurgy Institute **27**, 146 (2020).

[16] M. Ji, Y.H. Choa, Y.I. Lee, Ultrasonics Sonochemistry **74** (2021).

[17] A.P. Shpak, A.M. Korduban, M.M. Medvedskij, V.O. Kandyba, Journal of Electron Spectroscopy and Related Phenomena **156** (2007).

[18] Y. Badour, S. Danto, M. Gonidec, C. Labrugère, M.R. Suchomel, G. Philippot, M. Gaudon, Optical Materials **145** (2023).

[19] Y. Ye, H. Bai, M. Li, Z. Tian, R. Du, W. Fan, G. Xi, Advanced Materials Technologies **4**, 9 (2019).

[20] H. Tang, Z. Tang, J. Bright, B. Liu, X. Wang, G. Meng, N. Wu, ACS Sustainable Chemistry & Engineering **9**, 4 (2021).

[21] K. Shi, F. Wang, X. Li, W. Huang, K. Lu, K. Yang, Journal of Materials Science **58**, 16309 (2023).

[22] Z. Yang, J. Wang, J. Wang, M. Li, Q. Cheng, Z. Wang, X. Wang, J. Li, Y. Li, G. Zhang, Langmuir **38**, 1178 (2022).